

# Neural Stochastic Partial Differential Equations: Resolution-Invariant Learning of Continuous Spatiotemporal Dynamics

Cristopher Salvi<sup>1</sup> Maud Lemerrier<sup>2</sup> Andris Gerasimovičs<sup>3</sup>

## Abstract

*Stochastic partial differential equations* (SPDEs) are the mathematical tool of choice for modelling spatiotemporal PDE-dynamics under the influence of randomness. Based on the notion of mild solution of an SPDE, we introduce a novel neural architecture to learn solution operators of PDEs with (possibly stochastic) forcing from partially observed data. The proposed *Neural SPDE* model provides an extension to two popular classes of physics-inspired architectures. On the one hand, it extends Neural CDEs and variants – continuous-time analogues of RNNs – in that it is capable of processing incoming sequential information arriving irregularly in time and observed at arbitrary spatial resolutions. On the other hand, it extends Neural Operators – generalizations of neural networks to model mappings between spaces of functions – in that it can parameterize solution operators of SPDEs depending simultaneously on the initial condition and a realization of the driving noise. By performing operations in the spectral domain, we show how a Neural SPDE can be evaluated in two ways, either by calling an ODE solver (emulating a spectral Galerkin scheme), or by solving a fixed point problem. Experiments on various semilinear SPDEs, including the stochastic Navier-Stokes equations, demonstrate how the Neural SPDE model is capable of learning complex spatiotemporal dynamics in a resolution-invariant way, with better accuracy and lighter training data requirements compared to alternative models, and up to 3 orders of magnitude faster than traditional solvers.

## 1. Introduction

Motivated by the fact that many classical deep learning architectures may be interpreted as approximations to differential equations, there has been an increased interest in combining neural networks and differential equations into a hybrid approach, dubbed *neural differential equations* (Chen et al., 2018). When the data is sequential, recurrent neural networks (RNNs) and variants (GRU, LSTM etc.) are a popular modelling choice that can be regarded as a discrete approximation to some function of an underlying continuous signal.

*Neural controlled differential equations* (Neural CDEs) (Kidger et al., 2020) and variants<sup>1</sup> are the continuous-time analogue to RNNs. In essence, Neural CDEs embed a neural network  $f_\theta$  as the vector field of a differential equation  $dz_t = f_\theta(z_t)dX_t$  driven by a control path  $X_t$ , and the parameters  $\theta$  are then learnt from data so to optimize a given loss function. The term “ $dX_t$ ” means that the solution  $z_t$  of the equation (e.g. attention required from a doctor) can change in response to a change of an external stream of information  $\xi_t$  (e.g. heart rate of a patient). Despite offering many advantages for modelling temporal dynamics, Neural CDEs are not designed to process signals varying both in space and in time such as videos or physical fields arising from PDE-dynamics.

*Neural Operators* (Kovachki et al., 2021b) are generalizations of neural networks capable of modelling mappings between spaces of functions, therefore offering an attractive option for learning with spatiotemporal data. However, Neural Operators architectures generally fail to incorporate randomness into the systems they describe. In many cases the presence of noise leads to new phenomena, both at the mathematical and the physical level, often describing more complex and realistic dynamics than the ones arising from deterministic PDEs.

*Stochastic partial differential equations* (SPDEs) are the mathematical tool of choice to model many physical, biological and economic systems subject to the influence of randomness, be it intrinsic (e.g. quantifying uncertainty) or

<sup>1</sup>Imperial College London & The Alan Turing Institute, UK  
<sup>2</sup>University of Warwick, UK <sup>3</sup>University of Bath, UK. Correspondence to: Cristopher Salvi <csalvi@ic.ac.uk>.

<sup>1</sup>Neural SDEs (Kidger et al., 2021), Neural RDEs (Morrill et al., 2021).

extrinsic (e.g. modelling environmental random perturbations). Examples include the *Kardar–Parisi–Zhang (KPZ) equations* for random interface growth modelling, for instance, the propagation of a forest fire from a burnt region to an unburnt region (Hairer, 2013), the *Ginzburg–Landau equation* describing phase transitions of ferromagnets and superconductors (Temam, 2012), or the *stochastic Navier–Stokes equations* modelling the dynamics of a turbulent fluid flow under the presence of local random fluctuations (Mikulevicius & Rozovskii, 2004). For an introduction to SPDEs see Hairer (2009); a comprehensive textbook is Holden et al. (1996).

Similar to a *stochastic differential equations* (SDEs), the solution  $u$  to an SPDE is characterized by an initial condition  $u_0$  and a driving noise  $\xi$ . However, in the case of SDEs  $(u_0, \xi_t, u_t)$  are vectors, while in the case of SPDEs they are functions. Thus, Neural CDEs are not adapted to learn solution operators of SPDEs from data, due to the non-linear interactions between the various space-time points. While Neural Operators can model operators mapping the initial condition  $u_0$  or a realization of the forcing noise  $\xi$  to the solution  $u$  of a PDE, they offer no natural mechanism to handle SPDEs solution operators, where the solution  $u$  depends simultaneously on  $u_0$  and  $\xi$ .

## Contributions

Here we introduce the *neural stochastic partial differential equation* (Neural SPDE) model capable of learning solution operators of SPDEs of the form  $(u_0, \xi) \mapsto u$  from partially observed data. A Neural SPDE can be used to process (continuously in time) incoming sequential information arriving at an arbitrary spatial resolution. We propose two possible ways to evaluate a Neural SPDE, either by calling an ODE solver (emulating a spectral Galerkin scheme), or by solving a fixed point problem. We perform extensive experiments on various semilinear SPDEs, including the stochastic Ginzburg–Landau, Korteweg–De Vries and Navier–Stokes equations. The outcomes illustrate several aspects of our model: 1) it is space and time resolution-invariant, meaning that even if trained on a lower resolution it can be directly evaluated on a higher resolution; 2) it requires a lower amount of training data compared to alternative models; 3) for both choices of evaluation, it inherits memory-efficient backpropagation capabilities provided by existing adjoint-based and implicit-differentiation-based methods; 4) its evaluation is up to 3 orders of magnitude faster than traditional numerical solvers.

The outline of the paper is as follows: in Section 2 we provide a brief introduction to SPDEs which will help us to define our Neural SPDE model in Section 3. In Section 4 we present related work on Neural CDEs and Neural Operators, followed by numerical experiments in Section 5.

In Appendix A, we provide an overview of the computational aspects of SPDEs used to design the model and solve SPDEs numerically. Additional experiments can be found in Appendix B.

## 2. Background on SPDEs

Let  $T > 0$  and  $d, d_u, d_\xi \in \mathbb{N}$ . Let  $\mathcal{D} \subset \mathbb{R}^d$  be a bounded domain. Let  $\mathcal{H}_u = \{f : \mathcal{D} \rightarrow \mathbb{R}^{d_u}\}$  and  $\mathcal{H}_\xi = \{f : \mathcal{D} \rightarrow \mathbb{R}^{d_\xi}\}$  be two Hilbert spaces of functions on  $\mathcal{D}$  with values in  $\mathbb{R}^{d_u}$  and  $\mathbb{R}^{d_\xi}$  respectively.

We consider a large class of SPDEs of the type

$$du_t = (\mathcal{L}u_t + F(u_t)) dt + G(u_t)dW_t \quad (1)$$

where  $W_t$  is an infinite dimensional  $Q$ -Wiener process (Lord et al., 2014, Definition 10.6) or a cylindrical Wiener process (Hairer, 2009, Definition 3.54),  $F : \mathcal{H}_u \rightarrow \mathcal{H}_u$  and  $G : \mathcal{H}_u \rightarrow L(\mathcal{H}_\xi, \mathcal{H}_u)$  are two continuous operators<sup>2</sup>, and where  $\mathcal{L}$  is a linear differential operator generating a *semigroup*  $e^{t\mathcal{L}} : \mathcal{H}_u \rightarrow \mathcal{H}_u$ . For a primer on semigroup theory see Hairer (2009, Section 4).

A function  $u : [0, T] \rightarrow \mathcal{H}_u$  is defined to be a *mild solution* to the SPDE (1) if for any  $t \in [0, T]$  it satisfies

$$u_t = e^{t\mathcal{L}}u_0 + \int_0^t e^{(t-s)\mathcal{L}}F(u_s)ds + \int_0^t e^{(t-s)\mathcal{L}}G(u_s)dW_s$$

where the second integral is a stochastic integral (Hairer, 2009, Definition 3.57). An SPDE can be informally thought of as an SDE with solutions evolving in  $\mathcal{H}_u$  and driven by an infinite dimensional Brownian motion  $W$ . Assuming global Lipschitz regularity on  $F$  and  $G$ , a mild solution  $u$  to (1) exists and is unique (Hairer, 2009, Theorem 6.4) at least for short times.

In view of machine learning applications, one should think of  $W$  as a continuous space-time embedding of an underlying spatiotemporal data stream. In this paper we are only going to consider  $W$  to be a discretized sample path of a Wiener process, but we emphasise that the Neural SPDE model extends, in principle, beyond the scope of SPDEs and could be used for example to process videos in computer vision applications, which we leave as future work.

Computationally, it is reasonable to assume some degree of smoothness of  $W$ , at least at some local enough scale. As done in Kidger et al. (2020) for Neural CDEs, assuming differentiability of  $W$  in time, we can rewrite the mild solution of the Equation (1) as follows

$$u_t = e^{t\mathcal{L}}u_0 + \int_0^t e^{(t-s)\mathcal{L}}H_\xi(u_s)ds \quad (2)$$

<sup>2</sup> $L(\mathcal{H}_\xi, \mathcal{H}_u)$  denotes the space of bounded linear operators from  $\mathcal{H}_\xi$  to  $\mathcal{H}_u$ .

where  $H_\xi(u_t) := F(u_t) + G(u_t)\xi_t$  for  $\xi = \dot{W}$ . We also assume enough spatial regularity and take  $\mathcal{H}_u = L^2(\mathcal{D}, \mathbb{R}^{d_u})$  and  $\mathcal{H}_\xi = L^2(\mathcal{D}, \mathbb{R}^{d_\xi})$ . We will refer to  $\xi$  as white noise if is  $W$  a cylindrical Wiener process (see Appendix A.2 for further details on Wiener processes).

In the next section we introduce the Neural SPDE model.

### 3. Neural SPDEs

For a large class of differential operators  $\mathcal{L}$ , the action of the semigroup  $e^{t\mathcal{L}}$  can be written as an integral against a kernel function  $\mathcal{K}_t : \mathcal{D} \times \mathcal{D} \rightarrow \mathbb{R}^{d_u \times d_u}$  such that

$$(e^{t\mathcal{L}}h)(x) = \int_{\mathcal{D}} \mathcal{K}_t(x, y)h(y)\mu_t(dy), \quad (3)$$

for any  $h \in \mathcal{H}_u$ , any  $x \in \mathcal{D}$  and  $t \in [0, T]$ , and where  $\mu_t$  is a Borel measure on  $\mathcal{D}$ . As in Kovachki et al. (2021b), here we take  $\mu_t$  to be the Lebesgue measure on  $\mathbb{R}^d$  but other choices can be made, for example to incorporate prior information. We assume that  $\mathcal{K}$  is stationary so that Equation (2) can be rewritten in terms of the spatial convolution \*

$$u_t = \mathcal{K}_t * u_0 + \int_0^t \mathcal{K}_{t-s} * H_\xi(u_s)ds \quad (4)$$

In this work we propose two different ways of parameterizing the kernel  $\mathcal{K}$  and evaluating Equation (4); we will outline the details of both methods in Sections 3.2 and 3.3 below. For now, we will denote by  $\mathcal{K}_\theta$  either parameterization.

For a large class of SPDEs of the form (1), both  $F$  and  $G$  are local operators acting on a function  $h \in \mathcal{H}_u$ . In other words, the evaluations  $F(h)(x)$  and  $G(h)(x)$  at any point  $x \in \mathcal{D}$  only depend on the evaluation  $h(x)$  at  $x$ , and not on the evaluation  $h(y)$  at some other point  $y \in \mathcal{D}$  in the neighbourhood of  $x$ . This motivates the following model.

#### 3.1. The model

Let  $d_h > d_u$  be an integer,  $\mathcal{H}_h := L^2(\mathcal{D}, \mathbb{R}^{d_h})$  and let

$$\begin{aligned} L_\theta : \mathbb{R}^{d_u} &\rightarrow \mathbb{R}^{d_h}, & \Pi_\theta : \mathbb{R}^{d_h} &\rightarrow \mathbb{R}^{d_u}, \\ F_\theta : \mathbb{R}^{d_h} &\rightarrow \mathbb{R}^{d_h}, & G_\theta : \mathbb{R}^{d_h} &\rightarrow \mathbb{R}^{d_h \times d_\xi} \end{aligned}$$

be four feedforward neural networks. For any differentiable control  $\xi : [0, T] \rightarrow \mathcal{H}_\xi$ , define the map  $H_{\theta, \xi} : \mathcal{H}_u \rightarrow \mathcal{H}_u$

$$H_{\theta, \xi}(h)(x) = F_\theta(h(x)) + G_\theta(h(x))\xi_t,$$

for any  $h \in \mathcal{H}_u$ , any  $x \in \mathcal{D}$  and  $t \in [0, T]$ .

The *neural stochastic partial differential equation* (Neural SPDE) model is defined as follows:  $z_0(x) = L_\theta(u_0(x))$ ,

$$z_t = \mathcal{K}_{\theta, t} * z_0 + \int_0^t \mathcal{K}_{\theta, t-s} * H_{\theta, \xi}(z_s)ds \quad (5)$$

and  $u_t(x) = \Pi_\theta(z_t(x))$ , for any  $x \in \mathcal{D}$  and any  $t \in [0, T]$ . A schematic view of how Neural SPDEs can process spatiotemporal data is given in Figure 1. We note that globally Lipschitz conditions can be imposed by using, for example, ReLU or tanh activation functions in the neural networks  $F_\theta$  and  $G_\theta$ .

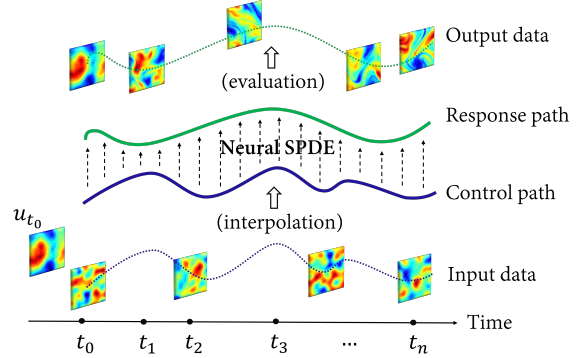


Figure 1. Schematic view of a Neural SPDE.

In the next two subsections we propose two numerical methods to evaluate the Neural SPDE model (5) yielding two different parameterization for the kernel  $\mathcal{K}$  in Equation (3).

#### 3.2. Kernel parameterization 1: ODE solver approach

Using the *convolution theorem* we can rewrite the integral in Equation (5) as follows

$$\begin{aligned} z_t = \mathcal{F}^{-1} &\left( \mathcal{F}(\mathcal{K}_t)\mathcal{F}(z_0) \right. \\ &\left. + \int_0^t \mathcal{F}(\mathcal{K}_{t-s})\mathcal{F}(H_{\theta, \xi}(z_s))ds \right) \end{aligned} \quad (6)$$

where  $\mathcal{F}, \mathcal{F}^{-1}$  are the  $d$ -dimensional Fourier transform (FT) and its inverse (see Definition A.1). Assuming that  $\mathcal{L}$  is a polynomial differential operator<sup>3</sup> of degree  $N$  of the form

$$\mathcal{L} = \sum_{n=0}^N \sum_{\substack{n_1, \dots, n_d \\ n_1 + \dots + n_d = n}} C_{n_1, \dots, n_d} \frac{\partial^n}{\partial x_1^{n_1} \dots \partial x_d^{n_d}},$$

where  $C_{n_1, \dots, n_d} \in \mathbb{C}^{d_h \times d_h}$  are complex matrices, then the FT of the kernel associated to  $\mathcal{L}$  satisfies

$$\mathcal{F}(\mathcal{K}_t)(y) = e^{tP(iy)} \in \mathbb{C}^{d_h \times d_h},$$

for any  $y \in \mathbb{C}^d$ , where  $e$  is the matrix exponential and  $P$  is the following matrix-valued polynomial

$$P(y) = \sum_{n=0}^N \sum_{\substack{n_1, \dots, n_d \\ n_1 + \dots + n_d = n}} (2\pi)^n y_1^{k_1} \dots y_d^{k_d} C_{n_1, \dots, n_d}$$

<sup>3</sup>This already contains a big class of SPDEs studied in physics. One could consider  $C_{n_1, \dots, n_d}$  to be a function of space for a more general setting.

This means that there exists a map  $A : \mathbb{C}^d \rightarrow \mathbb{C}^{d_h \times d_h}$  such that  $\mathcal{F}(\mathcal{K}_t)(y) = e^{tA(y)}$ . Thus, Equation (6) becomes

$$z_t = \mathcal{F}^{-1} \left( \underbrace{e^{tA} \mathcal{F}(z_0) + \int_0^t e^{(t-s)A} \mathcal{F}(H_{\theta,\xi}(z_s)) ds}_{:=v_t} \right)$$

where  $v_t : \mathbb{C}^d \rightarrow \mathbb{C}^{d_h}$  is the solution of the following ODE

$$\begin{aligned} \frac{dv_t}{dt} &= Av_t + \mathcal{F}(H_{\theta,\xi}(z_t)) \\ &= Av_t + \mathcal{F}(H_{\theta,\xi}(\mathcal{F}^{-1}(v_t))) \end{aligned}$$

Hence,  $z_t$  can be obtained by applying the inverse FT to the output of an ODE solver on  $[0, t]$  with initial condition  $\mathcal{F}(z_0)$ , vector field  $\Psi_{\theta,\xi} := A + \mathcal{F} \circ H_{\theta,\xi} \circ \mathcal{F}^{-1}$ , i.e.

$$z_t \approx \mathcal{F}^{-1}(\text{ODESolve}(\mathcal{F}(z_0), \Psi_{\theta,\xi}, [0, t]))$$

This approach can naturally be seen as a “neural version” of the classical *spectral Galerkin solver* for SPDEs described in Appendix A.3, with nonlinearities  $F, G$  and differential operator  $\mathcal{L}$  parameterized as outlined in this section.

We note that this numerical evaluation of the Neural SPDE model (5) allows to inherit memory-efficient adjoint-based backpropagation capabilities as in the evaluation of a Neural CDE. For further details on adjoint-based backpropagation we refer the reader to [Chen et al. \(2018\)](#).

### 3.3. Kernel parameterization 2: fixed point approach

In our second option of kernel parameterization, we will make use of three different versions of the FT: the time-only FT  $\mathcal{F}_1$  and its inverse  $\mathcal{F}_1^{-1}$ , the space-only FT  $\mathcal{F}_d$  and its inverse  $\mathcal{F}_d^{-1}$ , and the space-time FT  $\mathcal{F}_{d+1}$  and its inverse  $\mathcal{F}_{d+1}^{-1}$  (see Definition A.1). Denoting by  $\star$  the space-time convolution, the integral in Equation (5) can be rewritten as

$$z_t = \mathcal{K}_t \star z_0 + (\mathcal{K} \star \mathbb{1}_{\geq 0} H_{\theta,\xi}(z))_t$$

where  $\mathbb{1}_{\geq 0}$  is the indicator function restricting the temporal domain to the positive real line. Using again the convolution theorem we obtain

$$\begin{aligned} z_t &= \mathcal{F}_d^{-1}(\mathcal{F}_d(\mathcal{K}_t)\mathcal{F}_d(z_0)) \\ &\quad + \mathcal{F}_{d+1}^{-1}(\mathcal{F}_{d+1}(\mathcal{K})\mathcal{F}_{d+1}(\mathbb{1}_{\geq 0} H_{\theta,\xi}(z)))_t \end{aligned}$$

where all multiplications are matrix-vector multiplications.

Parameterizing  $\mathcal{F}_{d+1}(\mathcal{K})(y)$  directly in Fourier space as a complex tensor  $B$ , Equation (5) becomes

$$\begin{aligned} z_t &= \mathcal{F}_d^{-1}(\mathcal{F}_1^{-1}(B)_t \mathcal{F}_d(z_0)) \\ &\quad + \mathcal{F}_{d+1}^{-1}(B \mathcal{F}_{d+1}(\mathbb{1}_{\geq 0} H_{\theta,\xi}(z)))_t, \end{aligned}$$

where we used the fact that  $\mathcal{F}_d(\mathcal{K}_t) = \mathcal{F}_1^{-1}(\mathcal{F}_{d+1}(\mathcal{K}))_t$ . Hence, the solution  $z$  can be obtained by solving the fixed point problem  $z = \Phi_{\theta,\xi}(z)$ , where

$$\begin{aligned} \Phi_{\theta,\xi}(z)_t &:= \mathcal{F}_d^{-1}(\mathcal{F}_1^{-1}(B)_t \mathcal{F}_d(z_0)) \\ &\quad + \mathcal{F}_{d+1}^{-1}(B \mathcal{F}_{d+1}(\mathbb{1}_{\geq 0} H_{\theta,\xi}(z)))_t, \end{aligned}$$

This can be solved numerically by Picard’s iteration:

$$z \approx \text{FixedPointSolve}(z_0, \Phi_{\theta,\xi})$$

Analogously to adjoint-based backpropagation for the ODE solver approach mentioned in Section 3.2, there is a mechanism that leverages the *implicit function theorem* to back-propagate through the operations of a fixed point solver in a memory-efficient way. We refer the reader to [Bai et al. \(2019\)](#) for further details.

### 3.4. Space-time resolution-invariance

Let  $D = \{x_1, \dots, x_m\} \subset \mathcal{D}$  be a  $m$ -points discretization of the spatial domain  $\mathcal{D}$ , and let  $\mathcal{T} = \{t_0, \dots, t_n\} \subset [0, T]$  be a  $(n + 1)$ -points discretization of the time interval  $[0, T]$  with  $t_0 < \dots < t_n$ . As depicted in Figure 1, the input data corresponds to an irregularly sampled sequence of partially-observed spatial observations on the space-time grid  $D \times \mathcal{T}$ . The data is then interpolated to a continuous spatiotemporal signal  $\xi$  (and initial condition  $u_0$ ). By construction, the Neural SPDE model operates on the tuple of functions  $(u_0, \xi)$  to produce a spatiotemporal response  $u$ , also continuous in space and time; the function  $u$  can then be evaluated at an arbitrary space-time resolution (possibly different from  $D \times \mathcal{T}$ ) to produce the output data. Therefore, even if trained on a coarser resolution, a Neural SPDE can be directly evaluated on a finer resolution. In Section 5 we will demonstrate empirically this *zero-shot super-resolution* property of our model. We note that the FTs are numerically approximated using the *discrete Fourier transform* (DFT) and selecting a maximum number of frequency modes <sup>4</sup> (see Appendix A.1 for details).

Next, we provide a short overview of Neural CDEs and variants, and Neural Operators, both used as main benchmarks in the experimental section.

## 4. Related work

### 4.1. Neural CDEs, SDEs, RDEs

A *neural controlled differential equation* (Neural CDE), as popularised by ([Kidger et al., 2020](#)), is a parametric model

<sup>4</sup>The DFT approximates the Fourier series expansion truncated at a maximum number of modes. This allows to specify the shape of the two complex tensors  $A$  ( $k_{\max}^1 \times \dots \times k_{\max}^d \times d_h \times d_h$ ) in Section 3.2 and  $B$  ( $k_{\max}^1 \times \dots \times k_{\max}^{d+1} \times d_h \times d_h$ ) in Section 3.3. The  $k_{\max}^i$  are treated as hyperparameters of the model.



taking as input a time series interpolated into a continuous path  $X : [0, T] \rightarrow \mathbb{R}^{d_\xi}$  of bounded variation. The architecture of the model consists of a matrix-valued feedforward neural network  $f_\theta : \mathbb{R}^{d_h} \rightarrow \mathbb{R}^{d_h \times d_\xi}$  (satisfying some minimal Lipschitz regularity) parameterizing the vector field of the following dynamics

$$z_0 = \ell_\theta(u_0), \quad z_t = z_0 + \int_0^t f_\theta(z_s) dX_s, \quad u_t = \pi_\theta(z_t),$$

where  $\ell_\theta : \mathbb{R}^{d_u} \rightarrow \mathbb{R}^{d_h}$  and  $\pi_\theta : \mathbb{R}^{d_h} \rightarrow \mathbb{R}^{d_u}$  are feedforward neural networks. The output  $u_t$  is then fed to a loss function (mean squared, cross entropy etc.) and trained via stochastic gradient descent in the usual way. Depending on the regularity assumptions of the control  $X_t = \int_0^t \xi_s ds$ , the above integral can be interpreted as a Riemann–Stieltjes, a stochastic, or even a rough integral.

In the original version of Neural CDEs (Kidger et al., 2020),  $X$  is assumed differentiable and obtained via natural cubic splines interpolation of the original time series; therefore the term “ $dX_s$ ” can be interpreted as “ $\dot{X}_s ds$ ” and the integral can be evaluated numerically via a call to an ODE solver of choice (Euler, Runge-Kutta, adaptive schemes...).

*Neural stochastic differential equations* (Neural SDEs) are Neural CDEs where the control  $\xi$  is a sample path from a  $\mathbb{R}^{d_\xi}$ -dimensional Brownian motion; Neural SDEs can be used as generative models (trained either as VAEs or GANs) for time series (Kidger et al., 2021). In principal, Neural SPDEs could be used in an analogous way as the generator of a generative model for spatiotemporal data, provided one can construct a sensible notion of discrepancy on the relevant space of distributions for the discriminator (see Section 7).

*Neural rough differential equations* (Neural RDEs) (Morrill et al., 2021) generalize Neural CDEs in that they allow to relax the regularity assumption on  $X$  and consider a larger class of controls. In practice, Neural RDEs are particularly well suited for long time series. This is due to the fact that model can be evaluated via a numerical scheme from stochastic analysis (called the *log-ODE method*) over intervals much larger than what would be expected given the sampling rate or length of the time series. However, the space complexity of the numerical solver increases exponentially in the number of channels, thus model complexity becomes intractable for high dimensional time series.

## 4.2. Neural Operators

*Neural Operators* (Kovachki et al., 2021b; Li et al., 2020b;a) are generalizations of neural networks offering a way to model mappings between spaces of functions. Contrary to Neural CDEs, Neural Operators can be used to model mappings of the form  $u_0 \mapsto u$ , where  $u_0 : \mathcal{D} \rightarrow \mathbb{R}^{d_u}$  is the initial condition and  $u : \mathcal{D} \rightarrow \mathbb{R}^{d_u}$  is the solution of an

underlying PDE. Contrary to prior work attempting to merge PDEs and deep learning techniques, Neural Operators do not require knowledge of the exact form of the underlying PDE, they are resolution-invariant and they achieve superior performance compared to previous physics-inspired deep learning models.

Given an initial condition  $u_0$ , a Neural Operator with  $M$  layers is defined as follows

$$z^0 = L_\theta(u_0), \quad z^k = N_\theta^k(z^{k-1}), \quad u = \Pi_\theta(z^M),$$

for  $k = 1, \dots, M$ , and with feedforward neural networks  $L_\theta : \mathbb{R}^{d_u} \rightarrow \mathbb{R}^{d_h}$  and  $\Pi_\theta : \mathbb{R}^{d_h} \rightarrow \mathbb{R}^{d_u}$ . Each layer  $N_\theta^k$  is a parametric operator defined for any  $z : \mathcal{D} \rightarrow \mathbb{R}^{d_h}$  as

$$N_\theta^k(z) := \sigma \left( A_\theta^k z + b_\theta^k + \int_{\mathcal{D}} \mathcal{K}_\theta^k(\cdot, y) z(y) dy \right) \quad (7)$$

where  $A_\theta^k \in \mathbb{R}^{d_h \times d_h}$ ,  $b_\theta^k \in \mathbb{R}^{d_h}$ ,  $\mathcal{K}_\theta^k : \mathcal{D}^2 \rightarrow \mathbb{R}^{d_h \times d_h}$  is a matrix-valued kernel and  $\sigma$  is an activation function.

In the case of evolution-type PDEs, the solution  $u : [0, T] \times \mathcal{D} \rightarrow \mathbb{R}^{d_u}$  also depends on time. There are two ways of dealing with such time-dependent problems using Neural Operators. One can either consider  $\tilde{\mathcal{D}} = [0, T] \times \mathcal{D}$  as the new input domain, or use an auto-regressive structure in time to model the mapping  $z(t_{i-1}, \cdot) \rightarrow z(t_i, \cdot)$  as per (7). This allows to use Neural Operators for learning mappings of the form  $\xi \mapsto u$ , where  $\xi : [0, T] \times \mathcal{D} \rightarrow \mathbb{R}^{d_\xi}$  is a forcing term of the PDE. Among all kinds of Neural Operators, *Fourier Neural Operators* (FNOs) (Li et al., 2020c) stand out because of their easier parametrization while maintaining similar learning performance. The *Deep Operator Network* (DeepONet) (Lu et al., 2021) is another popular model for learning operators on function spaces that we use as an additional benchmark. For details on this model see Appendix B.1.

Despite their ability to model operators mapping either the initial condition  $u_0$  or a time-dependent forcing  $\xi$  to the solution  $u$  of a PDE, Neural Operators offer no natural mechanism to learn solution operators mapping the pair  $(u_0, \xi)$  to the solution  $u$ , which is crucial for solving SPDEs. Furthermore, as highlighted in the conclusion of Li et al. (2020c), in order to learn complex PDEs, Neural Operators require a large amount of training samples, which is a hard constraint for real-world applications as data generation is generally a very expensive procedure.

Neural CDE, Neural RDE, FNO and DeepONet will be the main benchmark models in our experimental section on semilinear SPDEs. Moreover, we propose an additional hybrid baseline consisting of a Neural CDE where the drift is modelled by an FNO and the diffusion by a feedforward neural network. The motivation for using a FNO to represent the drift comes from the approximation properties of FNOs

as detailed in [Kovachki et al. \(2021b\)](#), Theorem 4). We call the resulting model Neural CDE-FNO.

## 5. Experiments

In this section, we run experiments on three semilinear SPDEs: the stochastic Ginzburg-Landau equation in 5.1, the stochastic Korteweg-De Vries equation in 5.2, and the stochastic Navier-Stokes equations in 5.3. In particular we consider three supervised operator-learning settings:

- $u_0 \mapsto u$ , assuming the noise  $\xi$  is not observed;
- $\xi \mapsto u$ , assuming the noise  $\xi$  is observed, but the initial condition  $u_0$  is fixed across samples;
- $(u_0, \xi) \mapsto u$ , assuming the noise  $\xi$  is observed and  $u_0$  changes across samples.

We note that learning the operator  $u_0 \mapsto u$  of an SPDE without observing the driving noise  $\xi$  unavoidably yields poor results as only partial information about the system is provided as input to the models. However, we find informative to include the performances obtained in this setting, as this provides a sanity check that emphasizes the importance of the noise in all the experiments. Moreover, the ability to process the initial condition  $u_0$  on its own (in absence of noise) means that Neural SPDEs can be also used to learn deterministic PDEs. We provide an example on the deterministic Navier-Stokes equations in Appendix B.4.

For all the experiments, the loss function is the unnormalized pathwise  $L^2$  loss. The hyper-parameters for all the models were selected by grid-search (see Appendix B.1 for further experimental details). The code for the experiments is provided as supplementary material. We note that although the assumption of globally Lipschitz vector fields might be violated for the following SPDEs, well-posedness (i.e. existence of global solutions) can be shown using equation-specific arguments. Additional experiments may be found in Appendix B.

### 5.1. Stochastic Ginzburg-Landau equation

We start with a reaction diffusion equation in 1D called stochastic Ginzburg-Landau equation and given by

$$\begin{aligned}\partial_t u - \Delta u &= 3u - u^3 + \xi, \\ u(t, 0) &= u(t, 1), \\ u(0, x) &= u_0(x), \quad (t, x) \in [0, T] \times [0, 1]\end{aligned}$$

This equation is also known as the Allen-Cahn equation in 1-dimension and is used for modeling various physical phenomena like superconductivity ([Temam, 2012](#)). Here  $\xi$  denotes space-time white noise with sample paths generated using classical sampling schemes for Wiener processes described in Appendix A.2.

We consider two data-regimes: a *low data regime* where the total number of training observations is  $N = 1000$ , and a *large data regime* where  $N = 10000$ . In both cases, the response paths are generated by solving the SPDE along each sample path of the noise  $\xi$  using a finite difference scheme described in Appendix A.3 using 128 evenly distanced points in space and time and step size  $\Delta t = 10^{-3}$ . Following the same setup as in [Chevyrev et al. \(2021\)](#), equation (3.6)), we solve the SPDE until  $T = 0.05$  resulting in 50 time points and choose as initial condition  $u_0(x) = x(1 - x) + \kappa\eta(x)$ , where

$$\eta(x) = a_0 + \sum_{k=-10}^{k=10} \frac{a_k}{1 + |k|^2} \sin(k\pi x), \quad (8)$$

with  $a_k \sim \mathcal{N}(0, 1)$ .

We either take  $\kappa = 0$  or  $\kappa = 0.1$  to generate a dataset where the initial data is either fixed or varies across samples. We provide extra experiments on this SPDE for larger time horizons  $T$  and multiplicative forcing in Appendix B.2.

We report the results in Table 1. The Neural SPDE model (NSPDE) yields the lowest relative error for all tasks, reaching one order of magnitude improvement on the main task  $(u_0, \xi) \mapsto u$  in the large data regime compared to all the applicable benchmark models (NCDE, NRDE, NCDE-FNO). In all settings, even with a limited amount of training samples ( $N = 1000$ ), the NSPDE model is applicable and achieves  $\sim 1\%$  error rate, and marginally improves to  $< 1\%$  error when  $N = 10000$ .

### 5.2. Stochastic Korteweg-De Vries equation

Next, we consider a higher order SPDEs, namely the stochastic Korteweg-De Vries (KdV) equation given by

$$\begin{aligned}\partial_t u + \gamma \partial_x^3 u &= 6u \partial_x u + \xi, \\ u(t, 0) &= u(t, 1), \\ u(0, x) &= u_0(x), \quad (t, x) \in [0, T] \times [0, 1].\end{aligned}$$

This equation is used to describe the propagation of nonlinear waves at the surface of a fluid subject to random perturbations (another wave equation is studied in Appendix B.3). We refer the reader to [Wazwaz \(2009\)](#) for an overview on the KdV equation and its relations to solitary waves.

The stochastic forcing is given by  $\xi = \dot{W}$  for  $W$  being a partial sum approximation of a Q-Wiener process as per Example 10.8 in [Lord et al. \(2014\)](#) with  $\lambda_j \sim j^{-5+\varepsilon}$  and  $\phi_j(x) = \sin(j\pi x)$  (see Equation (10) in Appendix A.2). Taking small  $\varepsilon > 0$  guarantees that  $W_t$  is twice differentiable in space for every  $t \geq 0$ . To generate the datasets, we solve the SPDE with  $\gamma = 0.1$  until  $T = 0.5$ . The stochastic forcing is simulated using 128 evenly distanced points in space and a time step  $\Delta t_{\text{ref}} = 10^{-3}$ . We then approximate

**Table 1. Ginzburg-Landau equation.** We report the relative L2 error on the test set. The symbol x indicates that the model is not applicable. In the first task ( $u_0 \mapsto u$ ) only partial information ( $u_0$ ) is provided as input; the underlying noise  $\xi$  is used to generate the dynamics, it varies across samples, but is not provided as an input to the models. This explains why the performance of the applicable models (DeepONet, FNO and NSPDE) is poorer than for all other settings. In the second setting, ( $\xi \mapsto u$ ) the initial condition  $u_0$  is kept fixed. In the third setting, the initial condition  $u_0$  and the noise  $\xi$  change and are both provided as input.

Model	$N = 1\,000$			$N = 10\,000$		
	$u_0 \mapsto u$	$\xi \mapsto u$	$(u_0, \xi) \mapsto u$	$u_0 \mapsto u$	$\xi \mapsto u$	$(u_0, \xi) \mapsto u$
NCDE	x	0.112	0.127	x	0.056	0.072
NRDE	x	0.129	0.150	x	0.070	0.083
NCDE-FNO	x	0.071	0.066	x	0.066	0.069
DeepONet	0.130	0.126	x	0.126	0.061	x
FNO	0.128	0.032	x	0.126	0.027	x
NSPDE (Ours)	0.128	<b>0.009</b>	<b>0.012</b>	0.126	<b>0.006</b>	<b>0.006</b>

realizations of the solution of the KdV equation using a time step  $\Delta t = 10^{-2}$  until  $T = 0.5$ . Here, the initial condition is given by  $u_0(x) = \sin(2\pi x) + \kappa\eta(x)$ , where  $\eta$  is defined in Equation (8). Similarly to Section 5.1 we either take  $\kappa = 0$  or  $\kappa = 1$  to generate datasets where the initial condition is either fixed or varies across samples. Each dataset consists of  $N = 1\,000$  training observations.

As reported in Table 2, Neural SPDEs outperforms the second best model FNO by a full order of magnitude in the task  $\xi \mapsto u$  and the second best model NCDE-FNO by almost two orders of magnitude in the task  $(u_0, \xi) \mapsto u$ . We also perform the same tasks for a larger time horizons  $T = 1$  and report the results of a comparison against FNO in Table 3.

**Table 2. Stochastic KdV.** We report the relative L2 error on the test set. The symbol x indicates that the model is not applicable.  $N$  is fixed to 1 000 and  $T = 0.5$ .

Model	$u_0 \mapsto u$	$\xi \mapsto u$	$(u_0, \xi) \mapsto u$
NCDE	x	0.464	0.466
NRDE	x	0.497	0.503
NCDE-FNO	x	0.126	0.259
DeepONet	0.874	0.235	x
FNO	0.835	0.079	x
NSPDE (Ours)	0.832	<b>0.004</b>	<b>0.008</b>

**Table 3. Stochastic KdV with longer time horizon  $T = 1$ .**

Model	$u_0 \mapsto u$	$\xi \mapsto u$	$(u_0, \xi) \mapsto u$
FNO	0.913	0.112	x
NSPDE (Ours)	0.904	<b>0.009</b>	0.012

### 5.3. Stochastic Navier-Stokes equations

Finally, we consider the vorticity form of the Navier-Stokes equations in 2-dimensions for an incompressible flow

$$\begin{aligned} \partial_t w - \nu \Delta w &= -u \cdot \nabla w + f + \sigma \xi \\ w(0, x) &= w_0(x), \quad (t, x) \in [0, T] \times [0, 1]^2 \end{aligned} \quad (9)$$

where  $u$  is the unique divergence free ( $\nabla \cdot u = 0$ ) velocity field such that  $w = \nabla \times u$ . The Navier-Stokes equations describe the motion of incompressible fluid with viscosity  $\nu$  subject to the external forces (Temam, 2012). The deterministic forcing  $f$  is a function of space only and is defined as in Li et al. (2020c). The stochastic forcing  $\xi$  is given by  $\xi = \dot{W}$  for  $W$  being a Q-Wiener process which is colored in space and rescaled by  $\sigma = 0.05$  (see Appendix A.2). The initial condition  $w_0$  is generated according to  $w_0 \sim \mathcal{N}(0, 3^{3/2}(-\Delta + 49I)^{-3})$  with periodic boundary conditions. The viscosity parameter is set to  $\nu = 10^{-4}$ .

For each realization of the Q-Wiener process (sampled according to the scheme in Appendix A.2) we solve Equation (9) with a pseudo-spectral solver described in Appendix A.3, where time is advanced with a Crank–Nicolson update. We solve the SPDE on a  $64 \times 64$  mesh in space and use a time step of size  $10^{-3}$ . For the tasks  $u_0 \mapsto u$  and  $\xi \mapsto u$ , we generate the datasets by solving the SPDE up to time  $T = 1$  and downsample the trajectories by a factor of 10 in time (resulting in 100 time steps) and 4 in space (resulting in a  $16 \times 16$  spatial resolution). The number of training samples is  $N = 1\,000$ . To generate the training set for the task  $(u_0, \xi) \mapsto u$ , we generate 10 long trajectories of 15 000 steps each up to time  $T = 15$ . We partition each of these 10 trajectories into consecutive sub-trajectories of 500 time-steps using a rolling window. This procedure yields a total of 2 000 input-output pairs. We chose to split the data into shorter sequences of 500 time steps so that one batch training could fit in memory on a Tesla P100 NVIDIA GPU.

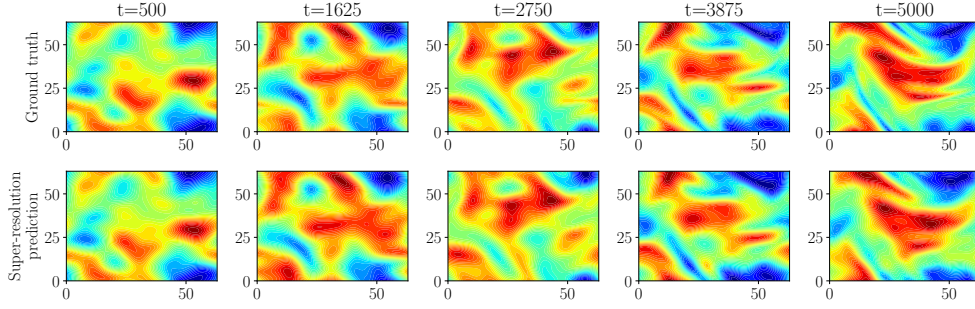


Figure 2. **Top panel:** Solution of the vorticity equation for one realisation of the stochastic forcing between the 500<sup>th</sup> and the 5 000<sup>th</sup> time steps. **Bottom panel:** Predictions with the Neural SPDE model given the initial condition at the 500<sup>th</sup> time step and the forcing between the 500<sup>th</sup> and the 5 000<sup>th</sup> time steps. The model is trained on a  $16 \times 16$  mesh and evaluated on a  $64 \times 64$  mesh.

Table 4. **Stochastic Navier-Stokes equations in two dimensions.**

We report the relative L2 error on the test set. The symbol x indicates that the model is not applicable. The symbol - indicates that the model does not fit in memory.

Model	$u_0 \mapsto u$	$\xi \mapsto u$	$(u_0, \xi) \mapsto u$
NCDE	x	0.366	0.843
NRDE	x	-	-
NCDE-FNO	x	0.326	0.178
DeepONet	0.432	0.348	x
FNO	0.188	0.039	x
NSPDE (Ours)	0.155	<b>0.034</b>	<b>0.049</b>

We report the results in Table 4. Neural SPDEs marginally outperforms FNO in the simpler task  $\xi \mapsto u$ , but with a significantly larger performance gap in the harder task  $(u_0, \xi) \mapsto u$  from the second best model NCDE-FNO. Figure 2 indicates that the Neural SPDE model is capable of zero-shot super-resolution in space and in time, achieving good performance even when evaluated on a larger time horizon of 5 000 time steps and on an upsampled  $64 \times 64$  spatial grid. Finally, we report in Table 5 the ratios of inference time of the trained Neural SPDEs over the runtime of the solvers, indicating that NSPDEs can be up to 3 orders of magnitude faster than traditional numerical solvers.

Table 5. Ratio of the inference time of NSPDE (once trained) over the runtime of the numerical solver for different SPDEs. In each case we consider a single solution. We use the same space and time discretization for both NSPDE and the numerical solver.

Dataset	Speedup
Stochastic Ginzburg-Landau Equation	59×
Stochastic Korteweg-De Vries Equation	80×
Stochastic Navier-Stokes	300×

## 6. Conclusion

We introduced the Neural SPDE architecture to learn solution operators of PDEs with (possibly stochastic) forcing from partially observed data. The proposed approach provides an extension to two popular classes of physics-inspired models. The model extends Neural CDEs, SDEs, RDEs in that it is resolution-invariant both in space and in time. It also extends Neural Operators as it can learn solution operators of SPDEs depending simultaneously on the initial condition and a realization of the driving noise. We performed extensive experiments on various semilinear SPDEs, including the stochastic Ginzburg-Landau, Korteweg-De Vries and Navier-Stokes equations. The outcomes illustrate the model achieves superior performance while requiring a lower amount of training data compared to alternative models, and its evaluation is up to 3 orders of magnitude faster than traditional numerical solvers.

## 7. Future work

Based on the promising empirical results obtained in this paper, we find the following to be interesting future research directions:

- use Neural SPDEs in computer vision applications for processing images and videos;
- construct a discrepancy between probability measures on spatiotemporal signals, generalizing for example the *signature kernel MMD* in Salvi et al. (2021). Neural SPDEs paired with such discrepancy would allow the design of new generative models for spatiotemporal signals generalizing the results in Kidger et al. (2021);
- prove universal approximation properties and derive error bounds for Neural SPDEs, similarly to the recent results in Kovachki et al. (2021a) for Neural Operators, possibly using tools from the theory of *regularity structures* (Hairer, 2014).



## References

- Alimov, S. A., Ashurov, R., and Pulatov, A. Multiple fourier series and fourier integrals. In *Commutative Harmonic Analysis IV*, pp. 1–95. Springer, 1992.
- Bai, S., Kolter, J. Z., and Koltun, V. Deep equilibrium models. *Advances in Neural Information Processing Systems*, 32:690–701, 2019.
- Briggs, W. L. and Henson, V. E. *The DFT: an owner’s manual for the discrete Fourier transform*. SIAM, 1995.
- Chen, R. T., Rubanova, Y., Bettencourt, J., and Duvenaud, D. Neural ordinary differential equations. In *Proceedings of the 32nd International Conference on Neural Information Processing Systems*, pp. 6572–6583, 2018.
- Chen, T. and Chen, H. Universal approximation to nonlinear operators by neural networks with arbitrary activation functions and its application to dynamical systems. *IEEE Transactions on Neural Networks*, 6(4):911–917, 1995.
- Chevryrev, I., Gerasimovics, A., and Weber, H. Feature engineering with regularity structures. *arXiv preprint arXiv:2108.05879*, 2021.
- Cooley, J. W. and Tukey, J. W. An algorithm for the machine calculation of complex fourier series. *Mathematics of computation*, 19(90):297–301, 1965.
- Hairer, M. An introduction to stochastic pdes. *arXiv preprint arXiv:0907.4178*, 2009.
- Hairer, M. Solving the kpz equation. *Annals of mathematics*, pp. 559–664, 2013.
- Hairer, M. A theory of regularity structures. *Inventiones mathematicae*, 198(2):269–504, 2014.
- Holden, H., Øksendal, B., Ubøe, J., and Zhang, T. Stochastic partial differential equations. In *Stochastic partial differential equations*, pp. 141–191. Springer, 1996.
- Kidger, P., Morrill, J., Foster, J., and Lyons, T. Neural controlled differential equations for irregular time series. *arXiv preprint arXiv:2005.08926*, 2020.
- Kidger, P., Foster, J., Li, X., Oberhauser, H., and Lyons, T. Neural sdes as infinite-dimensional gans. *arXiv preprint arXiv:2102.03657*, 2021.
- Kovachki, N., Lanthaler, S., and Mishra, S. On universal approximation and error bounds for fourier neural operators. *Journal of Machine Learning Research*, 22:Art–No, 2021a.
- Kovachki, N., Li, Z., Liu, B., Azizzadenesheli, K., Bhattacharya, K., Stuart, A., and Anandkumar, A. Neural operator: Learning maps between function spaces. *arXiv preprint arXiv:2108.08481*, 2021b.
- Li, Z., Kovachki, N., Azizzadenesheli, K., Liu, B., Bhattacharya, K., Stuart, A., and Anandkumar, A. Neural operator: Graph kernel network for partial differential equations. *arXiv preprint arXiv:2003.03485*, 2020a.
- Li, Z., Kovachki, N., Azizzadenesheli, K., Liu, B., Stuart, A., Bhattacharya, K., and Anandkumar, A. Multipole graph neural operator for parametric partial differential equations. *Advances in Neural Information Processing Systems*, 33, 2020b.
- Li, Z., Kovachki, N. B., Azizzadenesheli, K., Bhattacharya, K., Stuart, A., Anandkumar, A., et al. Fourier neural operator for parametric partial differential equations. In *International Conference on Learning Representations*, 2020c.
- Lord, G. J., Powell, C. E., and Shardlow, T. *An introduction to computational stochastic PDEs*, volume 50. Cambridge University Press, 2014.
- Lu, L., Jin, P., Pang, G., Zhang, Z., and Karniadakis, G. E. Learning nonlinear operators via deeponet based on the universal approximation theorem of operators. *Nature Machine Intelligence*, 3(3):218–229, 2021.
- Mikulevicius, R. and Rozovskii, B. L. Stochastic navier–stokes equations for turbulent flows. *SIAM Journal on Mathematical Analysis*, 35(5):1250–1310, 2004.
- Morrill, J., Salvi, C., Kidger, P., and Foster, J. Neural rough differential equations for long time series. In *International Conference on Machine Learning*, pp. 7829–7838. PMLR, 2021.
- Salvi, C., Cass, T., Foster, J., Lyons, T., and Yang, W. The signature kernel is the solution of a goursat pde. *SIAM Journal on Mathematics of Data Science*, 3(3):873–899, 2021.
- Temam, R. *Infinite-dimensional dynamical systems in mechanics and physics*, volume 68. Springer Science & Business Media, 2012.
- Wazwaz, A.-M. Solitary waves theory. In *Partial Differential Equations and Solitary Waves Theory*, pp. 479–502. Springer, 2009.

## Appendix

This appendix is organized as follows. In Appendix A we provide a summary of the computational aspects of SPDEs used for data simulation and model definition, emphasizing the important role of the Fourier Transform (A.1) for simulating noise realizations of Wiener processes (A.2) and building numerical solvers for SPDEs (A.3). In Appendix B we provide further experimental details (B.1) and additional experiments on the stochastic Ginzburg-Landau (B.2) and wave (B.3) equations, and on the deterministic Navier-Stokes PDE (B.4).

### A. Computational aspects of SPDEs

We start this section with the definition of the *Fourier Transform* (FT). We then define the *Discrete Fourier Transform* (DFT) as an approximation to the FT of a function observed at finitely many locations. Next, we discuss the role played by the FT to sample realizations of Wiener processes, necessary to build spectral solvers for SPDEs. The interested reader is referred to Briggs & Henson (1995) and Lord et al. (2014) for further details.

#### A.1. The Fourier Transform

Let  $V$  be a vector space over the complex numbers (e.g.  $\mathbb{C}^{d_h}$  or  $\mathbb{C}^{d_h \times d_h}$ ). Let  $r \in \mathbb{N}$  and let  $\mathcal{C} \subset \mathbb{R}^r$  be a compact subset of  $\mathbb{R}^r$ . In the paper we used either  $r = d$  and  $\mathcal{C} = \mathcal{D}$  or  $r = d + 1$  and  $\mathcal{C} = [0, T] \times \mathcal{D}$ .

**Definition A.1 ( $r$ -dimensional Fourier Transform).** The  $r$ -dimensional FT  $\mathcal{F}_r : L^2(\mathbb{R}^r, V) \rightarrow L^2(\mathbb{R}^r, V)$  and its inverse  $\mathcal{F}_r^{-1} : L^2(\mathbb{R}^r, V) \rightarrow L^2(\mathbb{R}^r, V)$  are defined as follows

$$\mathcal{F}_r(f)(y) = \int_{\mathbb{R}^r} e^{-2\pi i \langle x, y \rangle} f(x) dx, \quad \mathcal{F}_r^{-1}(g)(x) = \int_{\mathbb{R}^r} e^{2\pi i \langle x, y \rangle} g(y) dy$$

for any  $f, g \in L^2(\mathbb{R}^r, V)$ , where  $i = \sqrt{-1}$  is the imaginary unit and  $\langle \cdot, \cdot \rangle$  denotes the Euclidean inner product on  $\mathbb{R}^r$ .

In practice, we do not observe a function on  $\mathbb{R}^r$  but on a subset  $\mathcal{C} \subset \mathbb{R}^r$ . Furthermore, functions are observed at finitely many locations in  $\mathcal{C}$ , and another transform—the discrete Fourier transform (DFT)—is used for numerical computations.

In the sequel we denote by  $\Pi_N$  the set of periodic sequences indexed on  $\mathbb{Z}_r$  with period vector  $(N_1, \dots, N_r)$ .

**Definition A.2 ( $r$ -dimensional Discrete Fourier Transform).** The  $r$ -dimensional DFT  $\mathcal{D}_r : \Pi_N \rightarrow \Pi_N$  and its inverse  $\mathcal{D}_r^{-1} : \Pi_N \rightarrow \Pi_N$  are defined as follows,

$$\mathcal{D}_r(u)_n = \sum_{k \in \mathbb{Z}^r \cap \mathcal{R}_N} u_k e^{-2\pi i \langle n, N^{-1}k \rangle}, \quad \mathcal{D}_r^{-1}(v)_k = \frac{1}{|\det N|} \sum_{n \in \mathbb{Z}^r \cap \mathcal{R}_N} v_n e^{2\pi i \langle n, N^{-1}k \rangle}$$

with  $N = \text{diag}(N_1, \dots, N_r) \in \mathbb{N}^{r \times r}$ , and  $\mathcal{R}_N$  the rectangular domain  $\mathcal{R}_N = \{x \in \mathbb{R}^r \mid 0 \leq x_i < N_i, i = 1, \dots, r\}$ .

The DFT of a sequence can be computed exactly and efficiently using the *fast Fourier transform* (FFT) algorithm (Cooley & Tukey, 1965) which reduces the complexity from  $\mathcal{O}(M^2)$  to  $\mathcal{O}(M \log M)$  where  $M = N_1 N_2 \dots N_r$ . Most importantly, the FFT algorithm is implemented in machine learning libraries such as PyTorch, which provide support for GPU acceleration and automatic differentiation capabilities.

Note that if we have a finite sequence, we may still define its DFT by implicitly extending the sequence periodically. In particular, when a compactly supported function is sampled on its interval of support, and the samples are used as input for a DFT, it is as if the periodic extension of the function had been sampled. More precisely, consider an input sequence which corresponds to the evaluation of a function  $f$  on a regular grid of  $\mathcal{C} = \mathcal{R}_N$ . For simplicity, suppose that  $N_i = N_1$  for all  $i = 1, \dots, r$  and consider the grid points  $x_n = nL/N_1$  for  $n \in \mathbb{Z}^r \cap \mathcal{R}_N$ . Taking the DFT of the sequence of general term  $u_n = f(x_n)$  we obtain for all  $n \in \mathbb{Z}^r$ ,

$$\mathcal{D}_r(u)_n = \sum_{k \in \mathbb{Z}^r \cap \mathcal{R}_N} u_k e^{-2\pi i \langle n, k/N_1 \rangle} = \sum_{k \in \mathbb{Z}^r \cap \mathcal{R}_N} f(x_k) e^{-2\pi i \langle y_n, x_k \rangle},$$

where  $y_n$  are the reciprocal frequency points given by  $y_n = n/L$  for  $n \in \mathbb{Z}^r \cap \mathcal{R}_N$ . The DFT of a compactly supported (or approximately compactly supported) function  $f$  sampled on the regular grid of points  $x_k$  approximates the FT of  $f$  at the frequency points  $y_n$  (up to a constant multiplicative factor).

The FT is closely related to the notions of *Fourier coefficients* and *Fourier Series* defined hereafter.

**Definition A.3 ( $r$ -dimensional Fourier series).** Let  $f$  be a piecewise smooth function  $f : \mathbb{R}^r \rightarrow V$  which is periodic in  $x_i$  with period  $L_i \in \mathbb{R}_+$  for all  $i = 1, \dots, r$ . The  $r$ -dimensional Fourier series of  $f$  is a representation of the form,

$$f(x) \sim \sum_{n \in \mathbb{Z}^r} c_n(f) e^{2\pi i \langle L^{-1}n, x \rangle},$$

where  $L = \text{diag}(L_1, \dots, L_r) \in \mathbb{R}^{r \times r}$  and  $c_n(f)$  are complex coefficients, called *Fourier coefficients*, given by

$$c_n(f) = \frac{1}{|\det L|} \int_{\mathcal{R}_L} e^{-2\pi i \langle L^{-1}n, x \rangle} f(x) dx, \quad n \in \mathbb{Z}^r$$

where  $\mathcal{R}_L \subset \mathbb{R}^r$  denotes the rectangular domain of sides  $L_1, \dots, L_r$ .

We note that in the definition above, the sign  $\sim$  means that the series is a formal series and no statement is made about the convergence of the series (the forms of convergence are studied in [Alimov et al. \(1992\)](#)). If  $f$  is compactly supported on  $\mathcal{R}_L$ , we may still define its Fourier coefficients, and in this case  $\mathcal{F}_r(f)(y_n) = |\det L| c_n(f)$  at the frequency points  $y_n = L^{-1}n$ .

## Numerical consideration

Consider a function  $f$  which has compact support (or is periodic) which is observed at  $M$  locations in its support (or its unitary cell  $\mathcal{R}_L$ ). When using the DFT to approximate  $M$  points of the spectrum  $\mathcal{F}_r(f)(y_k)$  (or  $M$  coefficients  $c_k(f)$ ), a so-called *aliasing* error usually occurs: due to the periodicity of the DFT, the  $k^{\text{th}}$  coefficient of the DFT includes the contributions not only of the  $k^{\text{th}}$  frequency mode, but also from higher modes of the underlying function  $f$ . In general the accuracy of the highest frequency modes is more impacted by this error, and aliasing occurs specifically when we compute nonlinear terms in the physical space. For example, in the main paper we approximate the evaluation on the grid  $D \times \mathcal{T}$  of  $\mathcal{F}_{d+1}^{-1}(\mathcal{F}_{d+1}(\mathcal{K})\mathcal{F}_{d+1}(f))$  by  $\mathcal{D}_{d+1}^{-1}(B\mathcal{D}_{d+1}(f|_{D \times \mathcal{T}}))$  where  $f = \mathbb{1}_{\geq 0} H_{\theta, \xi}(z)$  and  $H_{\theta, \xi}$  is nonlinear. One possibility to mitigate aliasing is to set to zero the DFT terms (arising in nonlinearities) corresponding to the highest frequency modes before we apply the inverse DFT to go back to the physical space. This is precisely what we do when we parametrize only  $k_{\max}^1 \times \dots \times k_{\max}^{d+1} \times d_h \times d_h$  entries of the complex tensor  $B$ , and set the others to zero, hence resolving potential aliasing errors. We note that specific rules have been proposed (notably in the literature on pseudo-spectral solvers) to deal with specific nonlinearities. However, in the context of Neural SPDE we learn the nonlinearities, hence the number of frequency modes that we retain is treated as an hyperparameter.

## A.2. Stochastic simulation of Wiener processes

After defining Wiener processes we outline the sampling procedure that we used to simulate the datasets in the main paper. For more details on computational aspects of SPDEs the reader is referred to [Lord et al. \(2014\)](#).

Throughout this section,  $H$  will denote a separable Hilbert space (e.g.  $H = L^2(\mathcal{D})$ ) with a complete orthonormal basis  $\{\phi_k\}_{k \in \mathbb{N}}$ . Let  $(\Omega, \mathcal{F}, \mathcal{F}_t, \mathbb{P})$  be a filtered probability space.

### A.2.1. Q-WIENER PROCESS

Consider an operator  $Q : H \rightarrow H$  such that there exists a bounded sequence of nonnegative real numbers  $\{\lambda_k\}_{k \in \mathbb{N}}$  such that  $Q\phi_k = \lambda_k \phi_k$  for all  $k \in \mathbb{N}$  (this is implied by  $Q$  being a trace class, non-negative, symmetric operator, for example).

**Definition A.4 ( $Q$ -Wiener process).** Let  $Q$  be a trace class non negative, symmetric operator on  $H$ . A  $H$ -valued stochastic process  $\{W(t) : t \geq 0\}$  is called a  $Q$ -Wiener process if

1.  $W(0) = 0$  almost surely;
2.  $W(t; \omega)$  is a continuous sample trajectory  $\mathbb{R}^+ \mapsto H$ , for each  $\omega \in \Omega$ ;
3.  $W(t)$  is  $\mathcal{F}_t$ -adapted and has independent increments  $W(t) - W(s)$  for  $s < t$ ;
4.  $W(t) - W(s) \sim \mathcal{N}(0, (t - s)Q)$  for all  $0 \leq s \leq t$ .

In analogy to the Karhunen Loève expansion, it can be shown that  $W(t)$  is a  $Q$ -Wiener process if and only if for all  $t \geq 0$ ,

$$W(t) = \sum_{j=1}^{\infty} \sqrt{\lambda_j} \phi_j \beta_j(t) \tag{10}$$

where  $\beta_j(t)$  are i.i.d. Brownian motions, and the series converges in  $L^2(\Omega, H)$ . Moreover the series is  $\mathbb{P}$ -a.s. uniformly convergent on  $[0, T]$  for arbitrary  $T > 0$ . (i.e. converges in  $L^2(\Omega, \mathcal{C}([0, T], H))$ ).

In the Navier-Stokes example, we drive the SPDE by samples  $\xi$  from a  $Q$ -Wiener process in two dimensions. Here we follow Lord et al. (2014, Example 10.12) and explain how the sampling procedure works in this case. Let  $D = (0, L_1) \times (0, L_2)$  and consider an  $L^2(D)$ -valued  $Q$ -Wiener process  $W(t)$ . If the eigenfunctions of  $Q$  are given by,

$$\phi_k(x) = \frac{1}{\sqrt{L_1 L_2}} e^{2i\pi(k_1 x_1 / L_1 + k_2 x_2 / L_2)}$$

numerical approximation of sample paths from  $W(t)$  are easy to obtain through a DFT. Denote by  $\lambda_k$  the eigenvalues of  $Q$  (e.g.  $\lambda_k = e^{-\alpha|k|^2}$  for some parameter  $\alpha > 0$ ) and let  $\mathcal{J}$  be the index set defined by,

$$\mathcal{J} := \{(j_1, j_2) \in \mathbb{Z}^2 : -J_1/2 + 1 \leq j_1 \leq J_1/2, -J_2/2 + 1 \leq j_2 \leq J_2/2\}$$

The goal is to sample from the truncated expansion of  $W(t)$ ,

$$W^J(t) = \sum_{j \in \mathcal{J}} \sqrt{\lambda_j} \phi_j \beta_j(t),$$

at the collection of sample points,

$$x_k = (L_1 k_1 / J_1, L_2 k_2 / J_2)^T, \quad 0 \leq k_1 \leq J_1 - 1, 0 \leq k_2 \leq J_2 - 1.$$

Consider the random variable  $Z(t_n, x)$  defined by,

$$Z(t_n, x) = \sqrt{\Delta t} \sum_{j \in \mathcal{J}} \sqrt{\lambda_j} \phi_j(x) \xi_j^n, \quad \xi_j^n \sim \mathbb{CN}(0, 2),$$

meaning that  $\xi_j^n = a + ib$  with  $a, b \stackrel{\text{i.i.d.}}{\sim} \mathcal{N}(0, 1)$  such that  $Z(t_n, x_k)$  is a complex random variable with independent real and imaginary part with the same distribution as two independent copies of the increment  $W^J(t_n + \Delta t, x_k) - W^J(t_n, x_k)$ . Furthermore,  $Z(t_n, x_k)$  can be expressed in the form,

$$Z(t_n, x_k) = \frac{1}{J_1 J_2} \sum_{j_1 = -J_1/2 + 1}^{J_1/2} \sum_{j_2 = -J_2/2 + 1}^{J_2/2} \tilde{Z}_{j_1, j_2} e^{2i\pi(j_1 \frac{k_1}{J_1} + j_2 \frac{k_2}{J_2})} \quad (11)$$

where  $\tilde{Z}_{j_1, j_2} = \sqrt{\Delta t \lambda_{j_1, j_2}} J_1 J_2 \xi_{j_1, j_2}^n$ . We recognize that the matrix with entries given by Equation (11) is the 2D inverse DFT of the  $J_1 \times J_2$  matrix with entries  $\tilde{Z}_{j_1, j_2}$ . Therefore, we can sample two independent copies of

$$W^J(t_n + \Delta t, x_k) - W^J(t_n, x_k), \quad 0 \leq k_1 \leq J_1 - 1, 0 \leq k_2 \leq J_2 - 1$$

by computing a single 2D inverse DFT.

#### A.2.2. CYLINDRICAL WIENER PROCESS

If the operator  $Q = I$  is the identity, then  $Q$  is not of trace class on  $H$  so that the series in Equation (10) does not converge in  $L^2(\Omega, H)$ . This motivates the definition of cylindrical Wiener processes.

**Definition A.5 (Cylindrical Wiener process).** Let  $H$  be a separable Hilbert space. A cylindrical Wiener process (a.k.a space-time white noise) is a  $H$ -valued stochastic process  $\{W(t) : t \geq 0\}$  defined by

$$W(t) = \sum_{j=1}^{\infty} \phi_j \beta_j(t) \quad (12)$$

where  $\{\phi_j\}$  is any orthonormal basis of  $H$  and  $\beta_j(t)$  are i.i.d. Brownian motions.



In all examples except Navier-Stokes, we drive the SPDE by samples  $\xi$  from a cylindrical Wiener process in one dimension. Let  $D = (0, L)$  and consider an  $L^2(D)$ -valued cylindrical Wiener process  $W(t)$ . As explained in Lord et al. (2014, Example 10.31), if we take the basis

$$\phi_k(x) = \sqrt{2/L} \sin(k\pi x/L)$$

numerical approximation of sample paths from  $W(t)$  are easy to obtain. The goal is to sample from the truncated expansion,

$$W^J(t) = \sum_{j=1}^J \phi_j \beta_j(t), \quad (13)$$

at the collection of sample points  $x_k = kL/J$  for  $k = 1, \dots, J$ . Observing that a trigonometric identity yields,

$$\text{Cov}(W^J(t, x_i), W^J(t, x_k)) = (tL/J) \delta_{ik}, \quad i, k = 1, \dots, J$$

the increments  $W^J(t_n + \Delta t, x_k) - W^J(t_n, x_k) \sim \mathcal{N}(0, \Delta t L/J)$  for all  $k = 1, \dots, J$ .

### A.3. Numerical solvers

In this section we present an overview of the numerical solvers for SPDEs we used to generate the data for all the experiments. The stochastic Ginzburg-Landau (Section 5.1 and Appendix B.2), stochastic wave (Appendix B.3) equations have been solved using the finite difference method, while the stochastic Korteweg-De Vries (Section 5.2) and Navier Stokes (Section 5.3) equations have been solved using the spectral Galerkin method. We use the same setup as in Section 2. In particular, we focus on stochastic semilinear evolution equations of the form

$$du_t = (\mathcal{L}u_t + F(u_t))dt + G(u_t)dW_t \quad (14)$$

where  $W_t$  is either a  $Q$ -Wiener process or a cylindrical Wiener process and  $\mathcal{L}$  is a linear differential operator generating a semigroup  $e^{t\mathcal{L}}$ . We consider nonlinearities  $F, G$  regular enough (see Lord et al. (2014, Assumption 10.23)) to guarantee existence and uniqueness of mild solutions of Equation (14) (Lord et al., 2014, Theorem 10.26).

#### A.3.1. FINITE DIFFERENCE METHOD

We illustrate this numerical method for the reaction-diffusion equation

$$du_t = (\epsilon \partial_{xx}^2 u + F(u_t))dt + \sigma dW_t, \quad u(0, x) = u_0(x),$$

with homogeneous Dirichlet boundary conditions and where  $\epsilon, \sigma > 0$  are constants. We assume for simplicity that  $u_0, u_t, W_t$  are real-valued and  $\mathcal{D} = (0, a)$ . The generalization to higher dimensions is straightforward.

Consider the grid points  $x_j = jh$ , where  $h = \frac{a}{J}$  and  $j = 0, \dots, J$ , for some spatial resolution  $J \in \mathbb{N}$ . Let  $u_J(t)$  be the *finite difference approximation* of  $[u(t, x_1), \dots, u(t, x_{J-1})]$  (similarly for  $W_J(t)$ ) resulting from the solution of the following SDE

$$du_J(t) = [-\epsilon M u_J(t) + \hat{f}(u_J(t))]dt + \sigma dW_J(t)$$

where  $\hat{f}(u_J) = [f(u_1), \dots, f(u_{J-1})]^T$  and  $M$  is the  $(J-1) \times (J-1)$  matrix approximating Laplacian (with free boundary conditions) which is given by

$$M = \frac{1}{h^2} \begin{pmatrix} 2 & -1 & & & \\ -1 & 2 & -1 & & \\ & -1 & 2 & -1 & \\ & & \ddots & \ddots & \ddots \\ & & & -1 & 2 & -1 \\ & & & & -1 & 2 \end{pmatrix}$$

One could modify  $M$  for specific boundary conditions. For instance in the case of periodic boundary one should modify  $M_{1,J-1} = M_{J-1,1} = -1$  (see Lord et al. (2014, Chapter 3.4) for Dirichlet and Neuman boundary condition modifications of  $M$ ). To discretize in time, we may apply numerical methods for SDEs (see for example Lord et al. (2014, Chapter 8)). Choosing the standard Euler-Marayama scheme with time step  $\Delta t$  yields an approximation  $u_{J,n}$  to  $u_J(t_n)$  at  $t_n = n\Delta t$  defined by

$$u_{J,n+1} = (I + \Delta t \epsilon M)^{-1} \left( u_{J,n} + \hat{f}(u_{J,n}) \Delta t + \sigma (W_J(t_{n+1}) - W_J(t_n)) \right)$$

The increments  $(W_J(t_{n+1}) - W_J(t_n))$  are generated using techniques discussed in Appendix A.2.

### A.3.2. SPECTRAL GALERKIN METHOD

Consider again a separable Hilbert space  $H$ . Assume that the differential operator  $\mathcal{L}$  in Equation (14) has a complete set of orthonormal eigenfunctions  $\{\phi_j\}_{j \in \mathbb{N}}$  and eigenvalues  $\lambda_j < 0$ , ordered so that  $\lambda_{j+1} < \lambda_j$ . Then, we can define the semigroup  $e^{t\mathcal{L}}$  as follows

$$e^{t\mathcal{L}}h = \sum_{j=1}^{\infty} e^{\lambda_j t} \langle h, \phi_j \rangle \phi_j, \quad h \in H.$$

Define the *Galerkin subspace*  $V_J = \text{Span}\{\phi_1, \dots, \phi_J\}$  and the orthonormal projections  $P_J : H \rightarrow V_J$  as follows

$$P_J h = \sum_{i=1}^J \langle h, \phi_i \rangle \phi_i, \quad h \in H.$$

Then, the following defines *spectral Galerkin approximation* of Equation (14)

$$du_J(t) = (\mathcal{L}_J u_J(t) + P_J F(u_J(t)))dt + P_J G(u_J(t))dW_J(t), \quad u_J(0) = P_J u_0$$

where  $u_J := P_J u$  and  $\mathcal{L}_J := P_J \mathcal{L}$  and  $W_J = P_J W$  is as in (13). Using a Euler-Marayama discretization as above, we obtain the following discretization

$$u_{J,n+1} = (I + \Delta t \mathcal{L}_J)^{-1} (u_{J,n} + \Delta t P_J F(u_{J,n}) + P_J G(u_{J,n}) \Delta W_{J,n}).$$

This approach is particularly convenient for problems with additive noise where the eigenfunctions of  $\mathcal{L}$  and  $Q$  (the covariance of the  $Q$ -Wiener process  $W$ ) are equal, which is the case for all the experiments in this paper generated with this method. The eigenfunctions of the Laplacian with periodic boundary conditions correspond to the Fourier basis exponentials; therefore, one can define the projection  $P_J$  in terms of the DFT.

## B. Further experiments

We start this section with additional details on the training of NSPDE and the baseline models, including how the relevant hyperparameters have been selected for each model.

### B.1. Additional experimental details

For all experiments the dataset is split into a training, validation and test sets with relative sizes 70%/15%/15%. For all models, a grid search on the hyperparameters is performed using the training and validation sets. We use the Adam optimizer and a scheduler which reads the validation loss and reduces the learning rate if no improvement is seen for a *patience* number of epochs. Additionally, an early stopping method is used to halt the training of the model if no improvement is seen after a *patience* number of epochs. The hyperparameters included in the grid search are stated below and examples of hyperparameter selection results are provided in Tables 6 to 10.

**NSPDE** The hyperparameters included in the grid search are the number of frequency modes used to parametrize the kernel in Fourier space  $B = \mathcal{F}_{d+1}(\mathcal{K})$  and the number of forward iterations used to solve the fixed point problem.

**FNO** The hyperparameters included in the grid search are the number of frequency modes used to parametrize the kernel and the number of layers  $M$ . Note that the numbers of frequency modes in the grid search differ from the ones used for the NSPDE model by a factor 2 to ensure that the effective number of retained modes is the same. For both the NSPDE model and FNO, we kept the number of hidden channels fixed to  $d_h = 32$  as this systematically yielded better performances than previously included values and enabled to perform the grid search in a reasonable time.

**DeepONet** The *Deep Operator Network* (DeepONet) (Lu et al., 2021) is another popular class of neural network models for learning operators on function spaces. The DeepONet architecture is based on the universal approximation theorem of Chen & Chen (1995). It consists of two sub-networks referred to as the *branch* and the *trunk* networks. The trunk acts on the coordinates  $(t, x) \in [0, T] \times \mathcal{D}$ , while the branch acts on the evaluation of the initial condition  $u_0$  on a discretized grid  $D$ . Therefore, the DeepONet is not a space resolution-invariant architecture. The output of the network is expressed as

$$\text{DeepONet}(u_0)(t, x) = \sum_{k=1}^p b_k(u_0) \tau_k(t, x) + b_0,$$

where the  $b_k$  and the  $\tau_k$  are the outputs of the branch and trunk network respectively. The trunk network is usually a feedforward neural network, and one can chose the architecture of the branch network depending on the structure of the input domain. We follow [Lu et al. \(2021\)](#) and use feedforward neural networks for both the trunk and the branch networks. We perform a grid search on the depth and width of the trunk and branch feedforward neural networks.

**NRDE/NCDE/NCDE-FNO** The hyperparameters included in the grid search are the number of hidden channels and the type of solver as implemented by torchdiffeq ([Chen et al., 2018](#)). We note that we used a depth-2 NRDE model (depth-2 already results in  $d_\xi = 8385$  for forcings observed at 128 spatial points and higher depths models could not fit in memory) and recall that NCDE is a depth-1 NRDE.

Table 6. Grid search NCDE (KdV)

$d_h$	# parameters	solver	validation loss
8	136464	rk4	0.511
16	272672	rk4	0.510
32	545088	rk4	0.505
8	136464	euler	0.560
16	272672	euler	0.561
32	545088	euler	0.556

Table 7. Grid search NCDE-FNO (KdV)

$d_h$	# parameters	solver	validation loss
8	5761	rk4	0.140
16	15617	rk4	0.142
32	48769	rk4	0.145
8	5761	euler	0.310
16	15617	euler	0.314
32	48769	euler	0.321

Table 8. Grid search DeepONet (KdV)

Branch & trunk width	Branch depth	Trunk depth	# parameters	validation loss
256	3	4	1935616	0.258
128	3	4	885888	0.269
128	3	3	869376	0.279
128	3	2	852864	0.284
512	3	4	4526592	0.294
512	2	2	3738624	0.295
256	4	4	2001408	0.295
512	4	4	4789248	0.302
256	2	2	1738240	0.304
256	3	3	1869824	0.307
128	4	3	885888	0.311
128	4	2	869376	0.311
256	3	2	1804032	0.313
128	2	2	836352	0.315
256	4	2	1869824	0.316
128	4	4	902400	0.318
256	4	3	1935616	0.319
512	4	3	4526592	0.320
512	4	2	4263936	0.334
512	3	2	4001280	0.350
128	2	4	869376	0.350
512	3	3	4263936	0.359
512	2	3	4001280	0.366
256	2	3	1804032	0.370
128	2	3	852864	0.382
256	2	4	1869824	0.392
512	2	4	4263936	0.395

Table 9. Grid search FNO (KdV)

$d_h$	depth	modes 1	modes 2	# parameters	validation loss
32	1	16	16	532993	0.163
32	1	16	50	1647105	0.117
32	1	32	16	1057281	0.163
32	1	32	50	3285505	0.117
32	2	16	16	1058337	0.163
32	2	16	50	3286561	0.120
32	2	32	16	2106913	0.163
32	2	32	50	6563361	0.118
32	3	16	16	1583681	0.163
32	3	16	50	4926017	0.120
32	3	32	16	3156545	0.163
32	3	32	50	9841217	0.120
32	4	16	16	2109025	0.163
32	4	16	50	6565473	0.122
32	4	32	16	4206177	0.163
32	4	32	50	13119073	0.120

Table 10. Grid search NSPDE (KdV)

$d_h$	Picard's iterations	modes 1	modes 2	# parameters	validation loss
32	1	32	32	1055233	0.023
32	1	32	100	3283457	0.011
32	1	64	32	2103809	0.030
32	1	64	100	6560257	0.009
32	2	32	32	1055233	0.018
32	2	32	100	3283457	0.012
32	2	64	32	2103809	0.015
32	2	64	100	6560257	0.010
32	3	32	32	1055233	0.016
32	3	32	100	3283457	0.013
32	3	64	32	2103809	0.022
32	3	64	100	6560257	0.011
32	4	32	32	1055233	0.019
32	4	32	100	3283457	0.012
32	4	64	32	2103809	0.021
32	4	64	100	6560257	0.016

## B.2. Stochastic Ginzburg-Landau equation

Recall that the stochastic Ginzburg-Landau equations are of the form,

$$\begin{aligned} \partial_t u - \Delta u &= 3u - u^3 + G(u)\xi, \\ u(0, x) &= u_0(x), \quad (t, x) \in [0, T] \times [0, 1] \end{aligned} \tag{15}$$

subject to either Periodic or Dirichlet boundary conditions. Periodic boundary conditions are given by  $u(t, 0) = u(t, 1)$  for all  $t \geq 0$  and Dirichlet boundary conditions are given by  $u(t, 0) = u(t, 1) = 0$  for all  $t \geq 0$ . Initial condition we take as in Section 5.1  $u_0(x) = x(1 - x) + \kappa\eta(x)$  with  $\kappa = 0$  or  $\kappa = 0.1$  depending on a task. In both Periodic and Dirichlet case we can take  $\eta(x)$  as in (8) though in Dirichlet case one must take  $a_0 = 0$  to ensure  $u_0$  being zero at the boundary.



We first reproduce an experiment from Section 5.1 on the additive stochastic Ginzburg-Landau equation but with Dirichlet boundary conditions instead of the periodic. We compare it to the benchmark of FNO model which was the most successful among all the benchmarks of Section 5. From Table (11) we see that even though Neural SPDE model depends on the spectral methods the errors did not increase compared to the periodic equation in Section 5.1 (see Table 1). Our algorithm still outperforms FNO whose relative  $L_2$  error increased slightly. The fact that Neural SPDE can be applied to non-periodic equations could be perhaps explained by interpolation ( $L_\theta$ ) and projection ( $\Pi_\theta$ ) neural networks that could correct for non-periodicity of the data.

**Table 11. Additive stochastic Ginzburg-Landau equation with homogeneous Dirichlet boundary conditions.** The experimental setup is the same as in the main paper. We report the relative L2 error on the test set. The symbol x indicates that the model is not applicable.  $N$  is fixed to 1 000.

Model	$u_0 \mapsto u$	$\xi \mapsto u$	$(u_0, \xi) \mapsto u$
FNO	0.132	0.023	x
NSPDE (Ours)	0.135	0.008	0.010

We now take a look at the specific hyperparameter: number of forward iterations in the fixed point solver. We also call this a number of Picard iterations  $P$ . Theoretically as  $P$  increases Fixed Point Solver should converge to the true solution (see (Hairer, 2009)). This suggests that higher  $P$  should improve the performance of the Neural SPDE algorithms. In practise we observed in both additive Ginsburg Landau equation from Section 5.1 and in KdV equation from Section 5.2 that  $P = 1$  could already be enough. This could be explained either by dominance of the linear part of the equation or by overfitting in these cases. Thus we present an experiment on the multiplicative stochastic Ginzbug-Landau equation over a longer (compared to Section 5.1) time interval. In the Table 12 we compare NSPDE with  $P \in \{1, 2, 3, 4\}$  and again include FNO benchmark (which performed best in the previous experiments). We see that NSPDE with even  $P = 1$  outperforms FNO. Relative  $L_2$  error for  $T = 0.05$  increases for both NSPDE and FNO due to more complicated multiplicative noise. In Table 12 we present for each  $P$  the best result over other hyperparameters obtained by cross validation. One could clearly see an improvement in error as we increase the number of Picard iterations  $P$  (with an exception of the case  $T = 0.05$  where  $P = 3$  outperformed  $P = 4$ ). This improvement becomes more apparent as the time frame  $T$  increases. Heuristically (and qualitatively) this is due to the fact that for the short times solution of the SPDE is relatively close to its linearised version and that nonlinearity of the equation starts to play a bigger role for larger  $T$ .

**Table 12. Multiplicative stochastic Ginzburg-Landau equation.** We report the relative L2 error on the test for FNO and NSPDE (Ours) for different number of Picard iterations on the task  $\xi \rightarrow u$ .

Time horizon	FNO	NSPDE ( $P = 1$ )	NSPDE ( $P = 2$ )	NSPDE ( $P = 3$ )	NSPDE ( $P = 4$ )
$T = 0.05$	0.040	0.023	0.018	<b>0.016</b>	0.017
$T = 0.10$	0.068	0.042	0.041	<b>0.040</b>	<b>0.040</b>
$T = 0.25$	0.105	0.079	0.077	0.073	<b>0.072</b>

### B.3. The stochastic wave equation

In this section we consider the following nonlinear wave equation with multiplicative stochastic forcing,

$$\begin{aligned}
 \partial_t^2 u - \Delta u &= \cos(\pi u) + u^2 + u\xi, \\
 u(t, 0) &= u(t, 1), \\
 u(0, x) &= u_0(x), \\
 \partial_t u(0, x) &= v_0(x), \quad (t, x) \in [0, T] \times [0, 1].
 \end{aligned} \tag{16}$$

The nonlinear stochastic wave equation arises in relativistic quantum mechanics and is also used in simulations of nonlinear waves that are subject to either noisy observations or random forcing. We refer a reader to Temam (2012) for an overview

on the nonlinear wave equation. The above equation can put in a form of equation (1) by rewriting it as a system for  $(u, v) = (u, \partial_t u)$ . To generate training datasets, we solve the SPDE using a finite difference method with 128 evenly distanced points in space and a time step size  $\Delta t = 10^{-3}$ . As in [Chevyrev et al. \(2021, equation \(3.5\)\)](#), we solve the SPDE until  $T = 0.5$ . We then downsample the temporal resolution by a factor 5, resulting in 100 time points. Here, the initial condition is given by  $u_0(x) = \sin(2\pi x) + \kappa\eta(x)$ , where  $\eta$  is defined in Equation (8) and for simplicity initial velocity  $v_0$  is taken deterministic  $v_0(x) = x(1 - x)$ . Similarly to Section 5.1 we either take  $\kappa = 0$  or  $\kappa = 1$  to generate datasets where the initial condition is either fixed or varies across samples. Each dataset consists of  $N = 1\,000$  training observations.

**Table 13. Stochastic Wave equation.** We report the relative L2 error on the test set. The symbol x indicates that the model is not applicable.  $N$  is fixed to 1 000.

Model	$u_0 \mapsto u$	$\xi \mapsto u$	$(u_0, \xi) \mapsto u$
NCDE	x	0.142	0.432
NRDE	x	0.146	0.445
NCDE-FNO	x	0.029	0.037
DeepONet	0.190	0.143	x
FNO	0.151	0.026	x
NSPDE (Ours)	0.150	<b>0.023</b>	<b>0.026</b>

#### B.4. Deterministic Navier-Stokes PDE

In this final experiment, we demonstrate that our Neural SPDE model can also be used in the setting of PDEs without any stochastic term. We do so by studying the example from [\(Li et al., 2020c\)](#) on deterministic Navier-Stokes. More precisely, we consider the 2D Navier-Stokes equation for a viscous, incompressible fluid in vorticity form:

$$\partial_t w(t, x) - \nu \Delta w(t, x) = f(x) - u(t, x) \cdot \nabla w(t, x), \quad t \in [0, T], x \in [0, 1]^2 \quad (17)$$

$$\nabla \cdot u(t, x) = 0, \quad t \in [0, T], x \in [0, 1]^2 \quad (18)$$

$$w(x, 0) = w_0(x), \quad x \in [0, 1]^2 \quad (19)$$

where  $u : [0, T] \times [0, 1]^2 \rightarrow \mathbb{R}^2$  is the velocity field,  $w = \nabla \times u$  is the vorticity with  $w_0 : [0, 1]^2 \rightarrow \mathbb{R}$  being the initial vorticity. Here  $f$  is a deterministic forcing term which we take as in [\(Li et al., 2020c\)](#). We follow the experimental setup from [\(Li et al., 2020c\)](#) and use the dataset where  $\nu = 10^{-5}$ ,  $N = 1000$  and  $T = 20$ . We achieve similar performances as FNO with a L2 error of 0.17. A comparison between a true and predicted trajectory is depicted in Figure 3.

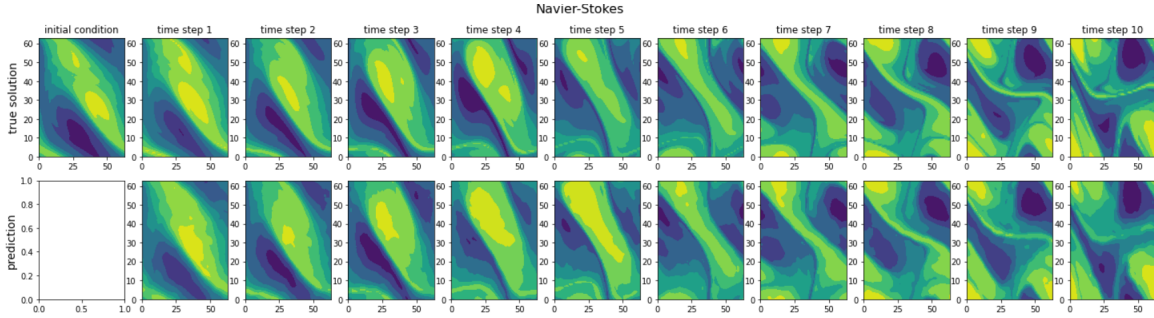


**Figure 3. Top panel:** Initial vorticity and ground truth vorticity at later time steps on a  $64 \times 64$  mesh. **Bottom panel:** Predictions of the Neural SPDE model.